MEASUREMENT OF THE ASYMMETRY IN CALORIMETER TRIGGERED HIGH-$P_\perp$ EVENTS USING A POLARIZED PROTON BEAM AND TARGET

E. Colton, R. Ditzler, D. Hill, H. Spinka, R. Stanek, K. Toshioka,
D. Underwood, R. Wagner, and A. Yokosawa
Argonne National Laboratory, Argonne, Illinois

Y. Hemmi, R. Kikuchi, K. Miyake, T. Nakamura, K. Nishimura and N. Tamura
Kyoto University, Kyoto, Japan

H. Azaïez, K. Kuroda, A. Michalowicz, D. Perret-Gallix
LAPP, Annecy, France

G. Shapiro
Lawrence Berekeley Laboratory
University of California, Berkeley, California

A. Kanofsky
Lehigh University, Bethlehem, Pennsylvania

L. Cormell, B. Robinson, W. Selove, G. Theodosiou
University of Pennsylvania, Philadelphia, Pennsylvania

M. Corcoran, H. E. Miettinen, T. A. Mulera, G. S. Mutchler,
G. C. Phillips, and J. B. Roberts
Rice University, Houston, Texas

A. DeLesquen and L. Van Rossum
Saclay, France

R. Brisa, F. Bradamante, S. Dalla Torre-Colautti, M. Giorgi, L. Lanceri,
A. Martin, P. Moras, A. Penzo, P. Schiavon and A. Villari
INFN, Sezione di Trieste, Trieste, Italy

A. Erwin and M. Thompson
University of Wisconsin, Madison, Wisconsin

January 30, 1981

European Spokesman:
L. Van Rossum
Saclay, France
(1) 941-8000

U.S. Spokesman:
R. Stanek
Argonne National Laboratory
FTS: 972-7616
Commercial (312

DIRECTOR'S OFFICE
FEB 3 1981

SUMMARY

We propose an experiment to measure asymmetries of events at high $p_\perp$ with opposite initial spin states. We will measure the single-spin asymmetry, A_N, where the beam is polarized in the transverse plane, and the double-spin asymmetry, A_{LL}, where both beam and target have longitudinal helicity. These asymmetry measurements will be done for single hadrons at high $p_\perp$ and also for jet-like events or clusters of particles at high $p_\perp$.

An existing calorimeter will be used to select jet events and also to simultaneously trigger on charged single hadrons. The use of a large aperture, magnetic spectrometer in the polarized beam line will aid in the reconstruction of the jet-like events to obtain a $p_\perp$ resolution of ± 0.35 GeV/c. A measurement of the asymmetries to ± 3% can be made at 400 GeV/c for jets at about $p_\perp$ = 6 GeV/c and for single hadrons at about $p_\perp$ = 4.5 GeV/c.

This experiment will attempt to shed more light on the current understanding of the basic hard scattering models as well as open the door to possible new horizons in polarization phenomena. The polarized beam at Fermilab provides an excellent opportunity to investigate spin effects as a natural and essential step for our further understanding of the constituent behavior.

We will run both with a liquid hydrogen target during the polarization measurements and later with a longitudinally polarized target. Proton induced reactions will be studied at 400 GeV/c and antiproton induced reactions at 200 GeV/c, where the $\bar{p}$ flux is highest.

I. Introduction

Since the observation of a strong s dependence and apparent power law $p_\perp$ dependence in high transverse momentum events, there has been a large investment of the high energy physics community in high $p_\perp$ reactions, on both experimental and theoretical scales. High $p_\perp$ reactions have helped develop the notions that constituents comprise hadrons and that it is these constituents which are fundamental in the high $p_\perp$ reactions. QCD has evolved into a probably correct theory to explain many aspects of high energy reactions. The unpolarized QCD theory successfully predicts many of the high $p_\perp$ observations.

The study of high $p_\perp$ reactions is not complete. Experimental problems with the definition of a jet make the jet properties vague. Much work is now going into an investigation of jet-jet correlations at various s and $p_\perp$ regions. The determination of quantum number flow from initial to final state using various beams is being pursued. Experimenters still need to find gluon jets in hadronic reactions. The theories still need to explain baryon production at large $p_\perp$ and the observed A^α dependence. All high $p_\perp$ information available will help theorists determine to what level the higher twist terms (CIM) are influencing the scattering processes. A detailed study is fundamental to our understanding of the hard scattering mechanism.

Along with the continuing struggle to interpret jet characteristics, further studies are necessary to obtain more insight into the hard scattering features. SLAC polarized electro-production data with polarized target are confirming theoretical beliefs that fast constituents within the proton are

retaining the characteristics of their parents' spin. This result implies that the spin is transmitted to the quarks which may then scatter in high $p_\perp$ reactions, transferring some component of spin to a final state hadron or jet.

Since a natural extension of jet studies is to understand the role of spin in the basic scattering process, we propose to measure spin asymmetries in high $p_\perp$ events using polarized p and $\bar{p}$ beams and a polarized nucleon target. These asymmetry measurements will provide further checks on the validity of QCD, which makes very definite predictions for single and double spin asymmetries. Besides QCD, we open up vast new horizons in exploring physics which has never been done before.

II. Physics Goals for High $p_\perp$ Experiments

The recent data on deep inelastic polarized ep scattering shown in Fig. 1[1] are considered evidence that large x quarks in the proton have a high probability of retaining the helicity of the parent proton. Since the only known way of studying parton-parton scattering is through the investigation of the properties of large transverse momentum hadron collisions, we can expect that the influence of constituent spins on the fundamental scattering processes may be of some consequence. A measurement of the asymmetries in $pp \to cX$ or $\bar{p}p \to cX$, with c a high $p_\perp$ hadron or a jet-like event, can be related to the fundamental $2 \to 2$ parton processes via the spin-weighted distribution functions[2-4] as shown in Fig. 2.

Unfortunately, deep inelastic electron production can only measure the spin dependence of quarks within the nucleon and therefore the spin properties of gluons within the proton are not yet established. But experiments are being proposed which will enable us to learn about the gluon polarization from asymmetry measurements in polarized J/ψ production. Gluons may be instrumental in jet production and in single particle triggers having $x_\perp \lesssim 0.3$.[2] Since the gluon fragmentation functions are expected to fall off faster at high z than the quark fragmentation functions, single particle triggers are "biased" in favor of quark decays while gluons are responsible for 70-80% of the jet triggers[2,5] at $x_\perp = 0.3$. At $x_\perp = 0.6$, gluons are estimated to cause 45% of the jets but only 3% of the single particle triggers. Thus for jet production and for single particles produced with $x_\perp \lesssim 0.3$, the subprocesses $qG \to qG$, $GG \to GG$ and $q\bar{q} \to GG$ are relatively more important than the subprocess $qq \to qq$. Asymmetry measurements where both the beam and target are polarized should provide new experimental information on the gluon spin distribution which cannot be probed directed in ep scattering. High $p_\perp$ events in polarized $\bar{p}p$ collisions allow us to compare $\bar{q}q \to GG$ with $GG \to GG$.

In pp collisions a K^- at high $p_\perp$ is preferentially produced by a quark scattered from the sea. The large Λ polarization observed at Fermilab and ISR[6] may be explainable by processes involving gluons or sea constituents which have a large polarization.[7] Comparing asymmetries for π and K production may also show interesting results on the relative polarization of the sea quarks.

Similarly, by comparing π^+ and π^- production at large $p_\perp$ the relative polarizations of u and d valence quarks can be estimated. For instance, first-order QCD indeed has very different predictions for the two-spin asymmetries A_{LL} for π^+ and π^- triggers, as seen in Fig. 4.

Single-spin asymmetries with only the beam polarized normal to the scattering plane will be measured; i.e.,

$$A_N \equiv P = \frac{Ed^3\sigma\uparrow/dp^3 - Ed^3\sigma\downarrow/dp^3}{Ed^3\sigma\uparrow/dp^3 + Ed^3\sigma\downarrow/dp^3}$$

for the process $p\uparrow p \to c + X$ with c a single hadron or jet at high $p_\perp$. The first-order QCD model predicts zero polarization, but experimental results showing up to 50% asymmetry[8] in the measurement of $pp\uparrow \to \pi^0 X$ (see Fig. 4) suggest extending this or similar measurements to higher energy. By using polarized beams and a hydrogen (or nuclear*) target the disadvantage of polarization dilution in polarized targets is avoided.

Recently progress has been made in understanding the observed $p_\perp$ behavior of inclusive hadron production at moderate values of $p_\perp$ within the framework of QCD.[10] This interesting result lends credence to the ideas that

* The non-trivial A-dependence of large $p_\perp$ hadron or jet production seen in unpolarized reactions is a clue that the fundamental scattering may not be incoherent. The study of the A-dependence of large $p_\perp$ production with polarized beams may clarify the nature of the A-dependence. Since the unpolarized A-dependence for jet and single particle production both show an anomaly[9], it may suffice to measure jet asymmetry in order to get to higher $p_\perp$. However, if no asymmetry is seen with jets, there may still be an effect in single particle production due to the lessened effect of gluons which may ultimately be unpolarized.

these processes can be described by a simple perturbative QCD approach. In this context, lowest order QCD makes very definite predictions on the spin-spin asymmetries of the basic $2 \to 2$ scattering (see Appendix 1). With a measurement of the double-spin asymmetry, A_{LL},

$$A_{LL}(s,x,p_\perp) = \frac{Ed^3\sigma(\overset{\rightarrow}{\leftarrow})/dp^3 - Ed^3\sigma(\overset{\rightarrow}{\rightarrow})/dp^3}{Ed^3\sigma(\overset{\rightarrow}{\leftarrow})/dp^3 + Ed^3\sigma(\overset{\rightarrow}{\rightarrow})/dp^3} ,$$

where $\rightleftarrows$ ($\rightleftarrows$) refers to parallel (anti-parallel) helicities, this experiment can provide valuable constraints on the relative contributions from different QCD subprocesses.

The asymmetry A_{LL} is predicted to be sizeable[4], ranging from 2% to 10% at $x_\perp = 0.5$ depending on the parton distributions used in the calculation. A_{LL} for both π° and jet triggers is shown is Fig. 5 for pp collisions and in Fig. 6 for $\bar{p}p$ collisions. The predicted A_{LL} for $\bar{p}p$ is smaller because the large $q\bar{q} \to GG$ process contributes a negative asymmetry.

The proposed experiment will be able to measure, with adequate statistics, the region out to $x_\perp = 0.4$ at $p_{lab} = 400$ GeV/c. Negative values for A_{LL} in pp collisions would seriously modify our understanding of the low order contributions to parton subprocessses, since all subprocesses $qq \to qq$, $qG \to qG$ and $GG \to GG$ contribute positive asymmetries. Large asymmetries would also contradict fundamental assumptions. If A_{LL} for $pp \to \text{Jet} + X$ is found to be positive while A_{LL} for $\bar{p}p \to \text{Jet} + X$ is negative, we can conclude that a large amount of $q\bar{q} \to GG$ contributes to jet production. We note that theoretically A_{NN}, when beam and target are polarized normal to the scattering plane, is expected to be negligible.[11]

The double-spin asymmetries we wish to measure for the single particle triggers are expected to be only weakly dependent on energy[3] above $\sqrt{s} = 20$ GeV and are maximum at $\theta_{c.m.} = 90°$, decreasing by only about 10% at $\theta_{c.m.} = 70°$.[4] We thus propose to measure the average of A_{LL} between $70° \lesssim \theta_{c.m.} \lesssim 110°$ and only at 400 GeV/c for incident protons and at 200 GeV/c for incident $\bar{p}$'s.

From the above discussion and weighted by the ease of performing certain measurements, we list in Table 1 an expected priority of experiments.

Table 1

Expected Experimental Measurements

Reaction	Measurement	Beam Polarization	Target
$pp \to h^{\pm}$, (jet-like) + X	$P = A_N$	$\vec{N}$	LH_2
$pp \to h^{\pm}$, (jet-like) + X	A_{LL}	$\vec{L}$	$\vec{L}$
$\bar{p}p \to h^{\pm}$, (jet-like) + X	A_{LL}	$\vec{L}$	$\vec{L}$
$pp \to h^{\pm}$, (jet-like) + X	A_{NN}	$\vec{N}$	$\vec{N}$

Note: h, (jet-like) means simultaneous measurements of single hadrons and jet-like events.

III. Design Features of the Experiment

In the proposed experiment, emphasis will not be on the rigorous definition of jet structure but in measuring the differences in cross section for different initial helicity states of high $p_\perp$ hadronic final states. This includes single particles of high $p_\perp$ and jet-like events, which we will consider as events consistent with what is presently known about jets. Our detector, therefore, must possess at least the following three capabilties:

1) It must be able to trigger efficiently and in an unbiased fashion on high $p_\perp$ jet-like events and single hadrons of large $p_\perp$ over a large kinematic region.
2) The transverse momentum of the jet or high $p_\perp$ hadron should be resolvable to within the resolution of our proposed bin width.
3) In order to reduce systematic errors, the triggering efficiency must be kept constant and uniform to a large degree. Alternatively, we will need to reverse beam and target polarizations frequently to average over any time dependent triggering inefficiencies. This reversal time should be much less than the time scale of variations within the detector.

Furthermore, these jet-like events can extend over a wide range of $p_\perp$ and center-of-mass angle. We will be interested in measuring events centered at 90°, where the asymmetry A_{LL} is predicted to be a maximum.

The conditions for selecting high $p_\perp$ jet-like events (condition 1) are the following:

a) The deposition of energy at angles about 90° c.m. must be large. We assume the large $p_\perp$ comes from a two-jet structure at ~ 90° CMS. This feature will be used in our Monte Carlo analysis, but it is not critical.

b) The energy distribution peaks in a small $\Delta\theta\Delta\phi$ region,

c) The energy distribution drops by a large factor before reaching the edge of the detector.

Parts (b) and (c) are necessary conditions to insure that our detector does not falsely create jet-like events. To select single hadrons at large $p_\perp$, the detector should have granularity in rapidity, allowing large energy deposition in a small Δy region. The ideal triggering detector is the highly segmented, good resolution hadron calorimeter designed and used by the Fermilab-Lehigh-Pennsylvania-Wisconsin group in Fermilab experiments E-395 and E-609.[12]

The calorimeter will be situated such that the entire azimuth will be covered between $70° \lesssim \theta_{c.m.} \lesssim 110^0$ as shown in Fig. 7. The angular acceptance of the calorimeter is shown in Fig. 8 for particles having $p_\perp < 0.5$ GeV/c and for particles with $p_\perp > 0.5$ GeV/c. The small block size of the calorimeter modules will enable us to sample small rapidity regions, $\Delta y \approx 0.4$, for the single particle trigger. The fine block system will also allow good energy resolution of the electromagnetic component of the jet events and, coupled with a large-aperture spectrometer as shown in Fig. 9, can determine both the neutral and charged component of the jet energy with better resolution than just the calorimeter alone.

It has been shown that a detector of finite size causes a bias in the selection of narrow jets.[13] Our detector, although of large solid angle, will not trigger on all jets, but only on a certain class of jet-like events. But for these events centered in the calorimeter, only ~ 10% of the triggering energy is contained outside 0.8 steradians[14] centered at 90° in the center-of-mass. This means that, for the sample of events centered at 90°, we can expect, on the average, to misjudge the jet $p_\perp$ by 0.3 - 0.4 GeV/c, essentially independent of $p_\perp$.[5,13,14] This uncertainty has also been verified in our Monte Carlo studies. Although our triggers and offline event reconstruction do not include all jet members, the systematic error in transverse momentum will be independent of beam or target polarizations.

We therefore conclude that for $p_\perp$ uncertainties of about ± 0.3 GeV/c in jet momentum, the E-609 calorimeter satisfies the criteria for efficiently triggering on jet-like events in an unbiased manner. Furthermore, with the proposed spectrometer, single charged hadrons will have their $p_\perp$ determined to better than ± 8%.

Uniformity of the calorimeter response from module to module is known to be better than ± 4%. Gain fluctuations of this magnitude are also expected with a time constant of about 24 hours. If the gain fluctuations, which cause varying triggering efficiencies, couple with beam or target spin reversal, then part of the asymmetry we measure will be due to the calorimeter fluctuations. Since good stability of the detector is not guaranteed, beam polarization should be reversed as often as possible, preferably every

spill. Similarly, to reduce systematic effects, the field of the analyzing magnet and the target polarization will be reversed every few hours.

A 2.5 meter long gas threshold Cerenkov counter will occupy the magnet volume. By using a radiator mixture of air and helium, $1.00029 < n < 1.00005$, we can select particular $p_\perp$ regions where we will be able to separate pions from kaons and protons (K/p's) for the single particle trigger (see section IV.D).

The polarized beam will be run at 3×10^7 protons/spill at 400 GeV/c with a 1/4 interaction length polarized Li^6D target. We will trigger simultaneously with a "single-particle" and a "global jet" trigger, both having more than one $p_\perp$ threshold. $\bar{p}$ induced jets will be studied at 200 GeV/c with an intensity of 3×10^6 antiprotons/spill. To get similar acceptance at 200 GeV/c, the calorimeters will have to be moved 30% closer to the target. This can be done by moving the polarized target closer to the magnet and moving the calorimeter and drift chambers upstream as far as they will go.

IV. Apparatus

A. Beam

The polarized beam line in the meson lab will be used. The characteristics of the beam are assumed to be those as detailed in Fermilab Proposal P-581. In particular, we assume

1) $\Delta p/p = 5\%$, divergence < 1 mrad,

2) Polarization $\approx 45\%$, longitudinal or transverse spin,

3) 3×10^7 protons/spill at 400 GeV/c and

3×10^6 antiprotons/spill at 200 GeV/c,

4) Tevatron II duty factors,

5) Beam size $\lesssim$ 2 cm diameter.

Beam hodoscopes of either narrow scintillator or proportional chambers will define the beam angle to ± 0.1 mrad ($\Delta p_\perp = \pm$ 0.04 GeV/c at 400 GeV/c). This measurement is important so that we are able to monitor beam position stability. A systematic change in beam direction, correlated with beam spin reversal, can create a false asymmetry, the magnitude of which depends on the relative triggering efficiency of the calorimeter modules.

To estimate the effects of beam motion we consider a systematic left-right beam divergence of 0.1 mrad and also assume that the left-right calorimeter efficiences differ by 5%. From the jet and single particle cross sections at 400 GeV/c,[15] we calculate a false asymmetry of < 0.6%. This number, of course, scales as the relative difference in detection efficiency.

Corrections to detector efficiency for varying instantaneous rates are important in the measurement of small asymmetries. This requires monitoring, and keeping constant, the instantaneous rates of beam and halo for opposite beam polarizations.

B. Target

The choice of polarized target is mainly dictated by the ability to attain large effective polarization, or equivalently, large signal to background. This requirement means that the degree of free nucleon polarization

should be high and that the number of polarizeable free nucleons to bound nucleons is large. Furthermore, for high $p_\perp$ events, the anomalous A^α effect enhances events from heavier, unpolarized nuclei in the target, causing a reduction in the effective polarization at high $p_\perp$. We therefore need the advantage of a target containing light elements which are not polarized.

We will use a Li^6D target which has an effective nucleon polarization of 33%, assuming no anomalous A dependence. The polarization per nucleon drops to about 22% when $\alpha = 1.5$. This material has a density of 0.58 gm/cm^3 and a free nucleon to bound nucleon ratio of 0.6. However, we note that Li^6D is an isoscalar target where both protons and neutrons are polarized.*

A 25% interaction length (20 cm) target with a diameter of 2 cm will be used. It will be polarized longitudinally in a superconducting solenoid magnet. The polarization will be reversed frequently as a consistency check on the data obtained by beam spin reversal and also as a crucial technique to eliminate systematic errors in the spin-spin measurements.

For the single-spin asymmetry measurements, we will use a liquid hydrogen target 2 cm in diameter by 100 cm in length (10% absorption length).

---

* In Section II we have discussed the double-spin asymmetry predictions for polarized proton targets. Although it is very appealing for comparison with theoretical ideas to use only protons as a target, isoscalar targets will introduce only isospin complications. In fact, A_{LL} will probably not change for $\vec{p}\vec{d} \to \text{Jet} + X$, but the neutron component in the target may make $A_{LL}(\vec{p}\vec{d} \to \pi^- + X) \simeq A_{LL}(\vec{p}\vec{d} \to \pi^+ + X)$. The isoscalar target should pose no problem to theorists interpreting the data.

C. Detectors

We intend to make use of a magnetic spectrometer as shown in Fig. 9. The spectrometer will give us additional information on the momentum of the particles comprising the jet and the momentum of single charged hadrons in the single-particle trigger. It will also be necessary to ascertain that all events come from within the target fiducial volume.

An analysis magnet with a low field integral will improve the charged particle momentum resolution over the calorimeter alone, but will not appreciably affect the trigger $p_\perp$. An SCM105, along with its power supply, will be supplied by Argonne. Shimming the pole pieces to 0.8 m vertical aperture still maintains relatively good field quality. The horizontal aperture of 2.1 m will not limit our θ acceptance out to $\sim 130°$ in the center-of-mass. With a $p_\perp$ kick of ~ 0.2 GeV/c, we can easily reconstruct momenta to the desired 8% resolution without significantly smearing the $p_\perp$ threshold and with a negligible dispersal of individual tracks.

Track detectors in front of the magnet will consist of both proportional chambers and drift chambers (P1, P2, D1, D2 in Fig. 9). The chambers from E-609 will be used, and in addition we will add a 1 mm proportional chamber, P1, just down stream of the target. This will add to the momentum resolution. A y coordinate in addition to those from E-609 will be added to the series of chambers in front of the magnet. It may be sufficient simply to use existing proportional chambers from Argonne as an aid to the track finding. P1 will be an xy chamber with 1 mm spacing, 13 cm x 13 cm active area, while P2 will be a 2 mm chamber measuring xuv coordinates and an active area

of 60 x 30 cm^2. D1 and D2 are drift chambers with active areas 120 x 60 cm^2 and 150 x 75 cm^2 respectively. Both chambers give two x coordinates each, but D2 will give a y coordinate from a delay line readout (resolution ≈ 1 cm). D1 has cells 1.2 and 3.2 cm and D2 has cells 2.4 and 3.2 cm.

In back of the magnet are drift chambers and proportional chambers, D3-D5 and P3. D3-D5 have 240 x 145 cm^2 active area; each gives two x coordinates, and D5 gives, via delay line, a y coordinate. The cell sizes for these chambers are 2.4 and 3.2 cm. Just in front of the calorimeter is a 2 mm PWC with active area 200 x 162 cm^2. In addition, it may be necessary to construct a y coordinate PWC or drift chamber to aid in reconstructing the tracks in back of the magnet. Studies are currently being done, and valuable advice will be obtained from the data from E-609.

A modification of some of the drift chamber electronics for use in high rates and for resolving left-right ambiguities may need to be done.

D. Cerenkov Counter

Charged hadron identification will be accomplished by means of a multi-celled gas threshold counter occupying the volume of the magnet (see Fig. 9). The main purpose of this counter is to tag the high $p_\perp$ single-particles as either pion or unresolved kaon or proton (K/p).

The counter will be 2.5 m long and have 16 cells, covering the angular range out to $\theta_{c.m.} \simeq 130°$. With wavelength shifters and bi-alkali photocathode photomultipliers, the counter will be capable of operation at the three photoelectron level with an effective index $(n-1) = 50 \times 10^{-6}$.

Figure 10 shows a plot of the allowed momentum of a particle with a given $p_\perp$ incident into the calorimeter. Also shown in the figure are the momenta where we can separate π's from K/p's with a 90% π detection efficiency. With a suitable mixture of air and helium, we can easily tune to a desired $p_\perp$ region and measure the asymmetry in π and K/p single-particle production. The gas proportions can be measured accurately with a laser interferometer.

E. Calorimeters

The calorimeter at the downstream end of the experiment consists of lead-scintillator sandwiches for electromagnetic detection and steel scintillator sandwiches for hadron detection. As shown in Fig. 7, we plan to use 108 of the E-609 calorimeter blocks - 40 modules 8" x 8", 48 modules 6" x 6" and 20 modules 4" x 4".

The calorimeter modules will be wired into a trigger matrix so that their output will be proportional to the energy deposited weighted by their mean lab angle ($p_\perp$). We intend to use the calorimeter subtending from 45° to about 130° in the center-of-mass, with a full 2π azimuthal coverage between $70° \lesssim \theta_{c.m.} \lesssim 112°$. It is important to have a uniform detector at opposite ϕ-angles to reduce false asymmetry measurements.

The tower construction of the calorimeter is schematically shown in Fig. 11. Each longitudinal segment contains two different types of modules: a 5 radiation length lead-scintillator sandwich (A') and three iron-scintillator sandwiches each 2 absorption lengths thick (A,B,C). The segments grow in transverse dimension with the development of the shower.

The A' modules, for electromagnetic detection, has 3 samplings of acrylic scintillator with three 1.0 cm Pb plates. The iron-scintillator modules, A, B and C, consist of either 16 iron plates, 2 cm thick, with 16 scintillator samples, or 20 iron plates, 1.3 cm thick and 20 scintillator samples. The modules with 20 samples are placed at larger lab angles in order to improve the energy resolution of the lower momentum particles. The calorimeter total thickness corresponds to 6.5 absorption lengths and 57 radiation lengths of material.

The energy resolution of the calorimeter was determined by E-395 to be

$$\frac{\Delta E}{E} = \frac{0.75}{\sqrt{E}} \quad \text{for hadrons}$$

$$= \frac{0.14}{\sqrt{E}} \quad \text{for electrons.}$$

From detailed studies and Monte Carlo calculations of E-395, a $p_\perp$ resolution of multi-particle groups is estimated to be ± 8%. This is within the uncertainty of the jet $p_\perp$.

V. Logistics

A. Triggers

With the large aperture calorimeter our triggers can be varied. The jet triggers can include a "jet-jet" trigger requiring a coincidence between two sides of the calorimeter. Such a trigger will eliminate the trigger bias caused by the Fermi motion of constituents inside the initial hadrons. Also

of interest is the "global" trigger created by looking at the total energy deposited in the calorimeter exceeding a preset threshold. The single jet trigger can also be used. We await the outcome of E-609 before deciding on a final "best" trigger to determine jets and minimize trigger biases.

The "single-particle" trigger will be a simultaneous, but distinct, trigger. The small block size of the calorimeters makes triggers by > 2 particles rather unlikely.

The trigger matrix which will allow us to use the outputs of all modules to form these varied triggers is now being constructed for E-609 and will be available for our use.

B. Rates

For the geometry described in Section IV we can estimate the yields from the observed single jet cross section and from the single particle cross section. The error in the asymmetry measurements for a total of N raw events (sum of both beam polarizations) is

$$\Delta A_N = \frac{1}{P_B} \frac{1}{\sqrt{N}} \quad \text{for single spin measurements}$$

$$\Delta A_{LL} = \frac{1}{P_B P_T} \frac{1}{\sqrt{N}} \quad \text{for double spin measurements.}$$

The number of events in a fiducial region between $p_\perp$ and $p_\perp + \Delta p_\perp$ is given by

$$N(p_\perp) = E \frac{d^3\sigma}{dP^3} \; 2\pi \cdot \Delta y \cdot \Delta\phi \cdot \Delta p_\perp \cdot p_\perp \cdot F$$

where $\Delta\phi$ is the fractional azimuthal acceptance and Δy is the rapidity acceptance. $\Delta p_\perp$ is the $p_\perp$ bin we choose. Since we cannot expect to measure the jets' $p_\perp$ to better than $\pm$ 0.3 GeV/c, we take $\Delta p_\perp$ = 0.75 GeV/c. For the single-particle trigger we are essentially limited by the spectrometer resolution for charged particles At $p_\perp$ = 4 GeV/c, a $\pm$ 8% resolution corresponds to $p_\perp$ = $\pm$ 0.32 GeV/c so that, for consistency, we also choose $\Delta p_\perp$ = 0.75 GeV/c. F is the target thickness multiplied by the beam flux.

The fiducial area used in these calculations corresponds to $70° < \theta_{c.m.} < 110°$, or $\Delta y = 0.73$. The full azimuth is used so $\Delta\phi = 1$. A flat x dependence is assumed. Table II lists the relative parameters for the beam and target for the single spin, A_N, and double spin, A_{LL}, measurements.

In order to estimate the effective target polarization, we can easily parameterize the A^α dependence of the target by assuming

$$p_{eff} \propto \frac{\rho_D}{\rho_D \cdot 2^{\alpha-1} + \rho_{Li} \cdot 6^{\alpha-1} + \rho_{He} \cdot 4^{\alpha-1}}$$

where the ρ_i's are the densities of the various target materials in Li^6D (~ 30% of the target volume is He^4). We obtain the approximate result for $1.0 \lesssim \alpha \lesssim 1.8$

$$p_T = 0.33 - (\alpha - 1)/4$$

for jet production[9] $\alpha(p_\perp) \simeq 1 + p_\perp/8$ while for single-particles above $p_\perp$ = 3 GeV/c, $\alpha(p_\perp) \simeq 1.1$.[15] This results in the approximate effective polarizations shown in Table II used in the rate calculations.

Table II

Parameters Assumed in Rate Calculation

	A_N	A_{LL}
Target	LH_2	Li^6D
Target length	100 cm	20 cm
Target density	0.72 g/cm^3	.58 g/cm^3
Effective target polarization	--	0.30 Single-particles 0.33 - $p_\perp$/32 Jets
Protons/hour at 400 GeV/c	1.8×10^9	1.8×10^9
Antiprotons/hour at 200 GeV/c	1.8×10^8	1.8×10^8
Beam polarization	0.5	0.5
$\Delta\phi\Delta y$	0.73	0.73
$\Delta p_\perp$	0.75 GeV/c	0.75 GeV/c

The cross sections can be written as

$$E \frac{d^3\sigma}{dp^3} = 10^{-28}\ 10^{-1.5(p_\perp - 3)}\ \text{mb/GeV}^2$$

for jets at 400 GeV/c and

$$E \frac{d^3\sigma}{dp^3} = \frac{15 \quad e^{-13x_\perp}}{(1 + p_\perp^2)^4} \text{ mb/GeV}^2$$

for single particle ($\pi^\pm$) triggers[16]. The 200 GeV/c jet cross sections are gotten from Bromberg et al.[5] and we assume $\sigma(\bar{p}p) = \sigma(pp) = \sigma(pn) = \sigma(\bar{p}n)$ for both jets and π's.

Assuming 100% operating efficiency, the expected errors on A_N for 50 hours of running and for A_{LL} for 350 hours of running are listed in Tables III and IV.

Table III

Error in A_N for 50 Hours of Beam on Target

	200 GeV/c		400 GeV/c	
$p_\perp$ (GeV/c)	$\bar{p}p \to$ Jet X ΔA_N(%)	$\bar{p}p \to \pi^\pm$ X ΔA_N(%)	$pp \to$ Jet X ΔA_N(%)	$pp \to \pi^\pm$ X ΔA_N(%)
3	.34	4.85	.03	.85
4	1.46	23.8	.12	3.4
5	6.5	--	.62	11.5
6	29.5	--	3.2	--
7	--	--	16.7	--

Table IV

Error In A_{LL} for 350 Hours of Beam on Target

	200 GeV/c		400 GeV/c	
$p_\perp$ (GeV/c)	$\bar{p}N \to$ Jet X $\Delta A_{LL}(\%)$	$\bar{p}N \to \pi^\pm$ X $\Delta A_{LL}(\%)$	pN → Jet X $\Delta A_{LL}(\%)$	pN → $\pi^\pm$ X $\Delta A_{LL}(\%)$
3	.17	1.95	.01	.34
4	.86	9.5	.07	1.4
5	4.5	--	.43	4.6
6	24.8	--	2.7	13.7
7	--	--	17.8	--

In the rate calculations for π production we assume the same fiducial region as with the jet trigger. But in actuality we would use the entire calorimeter region, $45° \lesssim \theta_{c.m.} \lesssim 125^0$. The increased acceptance results in a 50% reduction in the asymmetry errors for the same running period. Also, for charged hadron asymmetry measurements, the errors for charged single particles will, of course, be less than the π errors listed in the tables.

B. Run Plan

We request a total of 1000 hours to complete the following measurements:

System check out and calibration:	150 hours (parasite)
Polarization at 400 GeV/c:	50 hours
Polarization at 200 GeV/c:	50 hours
Spin-spin asymmetry at 400 GeV/c:	375 hours
Spin-spin asymmetry at 200 GeV/c:	375 hours

At 400 GeV/c, this would provide an A_{LL} measurement to ± 3% for jets having $p_\perp \lesssim 6$ GeV/c and single particles with $p_\perp \lesssim 4.5$ GeV/c. Likewise, polarization can be measured with an accuracy of ± 3% at a jet $p_\perp \lesssim 6$ GeV/c and single particle $p_\perp \lesssim 4.5$ GeV/c.

References

1. M. J. Alguard et al., Phys. Rev. Lett. 37, 1258 (1976); Phys. Rev. Lett. 37, 1261 (1976); Phys. Rev. Lett. 41, 70 (1978); Madison Conference, 1980.

2. R. P. Feynman, R. D. Field and G. C. Fox, Nucl. Phys. B128, 1 (1977); Phys. Rev. D18, 3320 (1978).

3. R. D. Field, ANL Preprint ANL-HEP-CP-77-45 (June, 1977); J. Ranft and G. Ranft, Phys. Lett. 77B, 309 (1978); H. Cheng and E. Fischbach, Phys. Rev. D19, 860 (1979).

4. J. Babcock, E. Monsay and D. Sivers, Phys. Rev. Lett. 40, 1161 (1978); Phys. Rev. D19, 1483 (1979).

5. C. Bromberg et al., Nucl. Phys. B171, 1 (1980).

6. G. Bunce et al., Phys. Rev. Lett. 36, 1113 (1976); K. H. Heller et al., Phys. Lett. 68B, 480 (1977) and Phys. Rev. Lett. 41, 607 (1978); S. Erhon et al., Phys. Lett. 82B, 301 (1979); F. Lomanno et al., Phys. Rev. Lett. 43, 1905 (1979); K. Raychaudhuri et al., Phys. Lett. 90B, 319 (1980).

7. K. Heller, University of Michigan Report No. UM HE77-38, 1977; G. Kane and Y. P. Yao, Nucl. Phys. B137, 313 (1978); B. Anderson et al., Phys. Lett. 85B, 417 (1979).

8. J. Antille et al., Phys. Lett. 94B, 523 (1980).

9. C. Bromberg et al., Kaysersberg Conference (1977) and Phys. Rev. Lett. 42, 1202 (1979).

10. For a comprehensive review, see M. Jacob, EPS International Conference on High Energy Physics, Geneva 1979 (CERN, Geneva, 1979) Vol. 2, 473 and R. Field, Proc.XIX Int.l Conf. on High Energy Physics, Tokyo, Japan (1978).

11. K. Hidaka, E. Monsay and D. Sivers, Phys. Rev. D19, 1503 (1979).

12. M. D. Corcoran et al., Fermilab Proposals 395 and 609; B. T. Yost et al., IEEE Transactions on Nuclear Science, Vol. NS-26, No. 1, p 105 (1979); W. Selove et al., Proceedings of the Calorimeter Workshop, 1975, editor M. Atac (Fermilab, Batavia, 1975).

13. M. Dris, Nucl. Instr. and Meth. 158, 89 (1979).

14. W. Selove, Proc of the XIVth Rencontre de Moriond, edited by J. Tran Thanh Van, Vol. 1, p. 401 (1979).

15. D. Antreasyan et al., Phys. Rev. D19, 764 (1979).

16. L. Cormell et al., Evidence for Jets, and for Correlated Jets, in High $p_\perp$ Events, University of Pennsylvania Report UPR-24E, October 1977 (unpublished); J. A. Appel et al., Phys. Rev. Lett. 33, 719 (1974).

Figure Captions

Figure 1 Experimental values of $(\sigma_{1/2} - \sigma_{3/2})/(\sigma_{1/2} + \sigma_{3/2})$ vs. x. $\sigma_{1/2}(\sigma_{3/2})$ is the total absorption cross section when the z component of angular momentum of the photon plus proton is 1/2 (3/2).

Figure 2 Hard scattering model for initially polarized protons with helicities λ_A and λ_B.

Figure 3 The measured asymmetry in $pp\uparrow \rightarrow \pi^0 + X$ as a function of $p_\perp$ in the Feynman x range 0-0.1. Data is from Ref. 8.

Figure 4 Asymmetry, A_{LL}, for the reaction $pp \rightarrow \pi^\pm + X$ as a function of $x_\perp$ for (a) conservation SU(6) distributions,
(b) diquark distributions, and
(c) Carlitz-Kaur distributions.

Figure 5 Asymmetry, A_{LL}, for reactions $pp \rightarrow (\pi^0 \text{ or Jet}) + X$ as a function of $x_\perp$ for
(a) conservative SU(6) distributions,
(b) diquark distributions, and
(c) Carlitz-Kaur distributions.

Figure 6 Asymmetry, A_{LL}, for reactions $\bar{p}p \rightarrow (\pi \text{ or Jet}) + X$ as a function of $x_\perp$ for

(a) conservative SU(6) distributions,

(b) diquark distributions, and

(c) Carlitz-Kaur distributions.

Figure 7 The structure of the front face of the calorimeter and the angular regions covered at 400 GeV/c. Note full azimuthal acceptance in the range $65° \lesssim \theta_{c.m.} \lesssim 112^0$.

Figure 8 The calorimeter angular acceptance 400 GeV/c for particles having $p_\perp < 0.5$ GeV/c and for particles having $p_\perp > 0.5$ GeV/c.

Figure 9 Plan view of the spectrometer. P1-P3 are proportional chambers and D1-D5 are drift chambers. The calorimetries, EC and HC, are shown subtending the region $\theta_{c.m.} \lesssim 110^0$. Not shown is the beam polarimeter downstream of the calorimeter.

Figure 10 p vs $p_\perp$ for hadrons between 70° and 110° in the center of mass. Also shown (arrows) are the regions where a K/p and π can be separated with 90% π detection efficiency using a suitable mixture of helium and air.

Figure 11 A schematic view of the E609 calorimeter showing the tower construction.

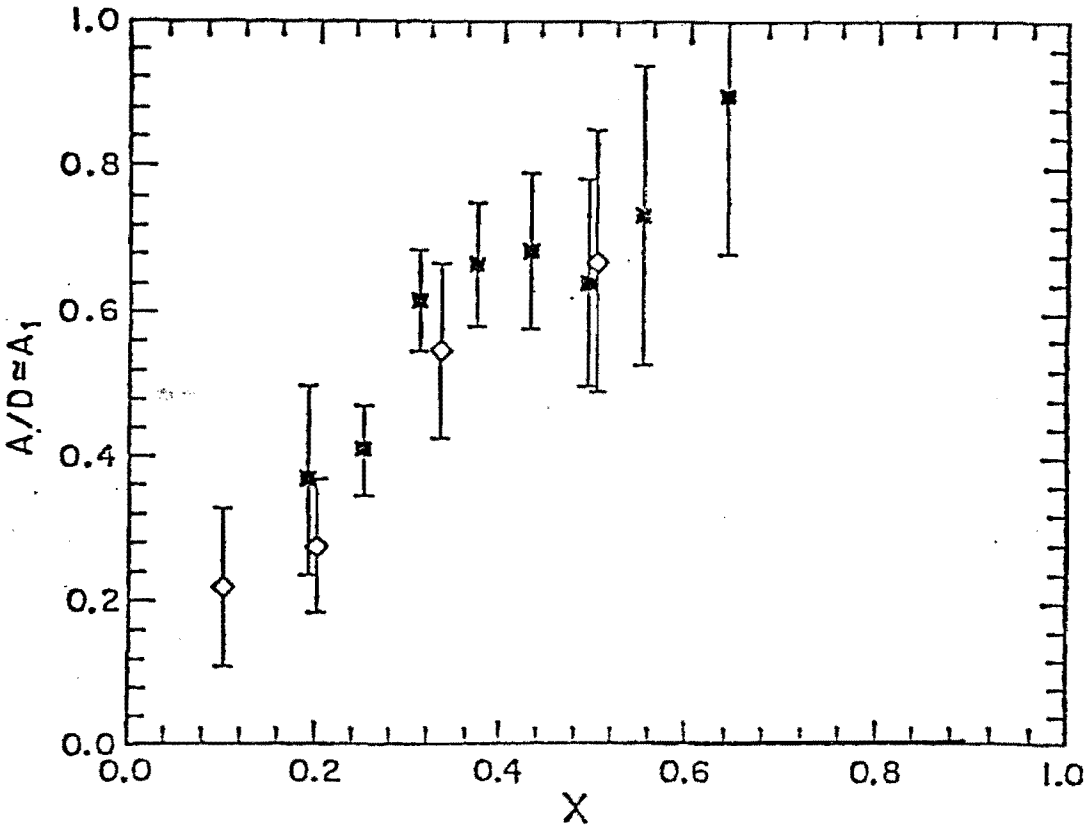

Figure 1

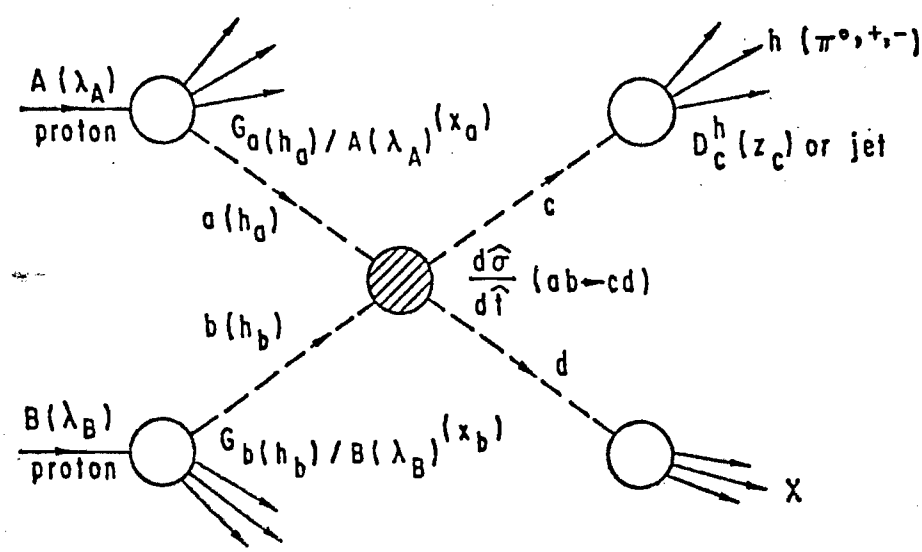
A (λA)
proton
Ga(ha) / A(λA)(xa)
a (ha)
b (hb)
B(λB)
proton
Gb(hb) / B(λB)(xb)
h (π°,+,-)
Dhc (zc) or jet
c
dσ̂/dt̂ (ab→cd)
d
X

Figure 2

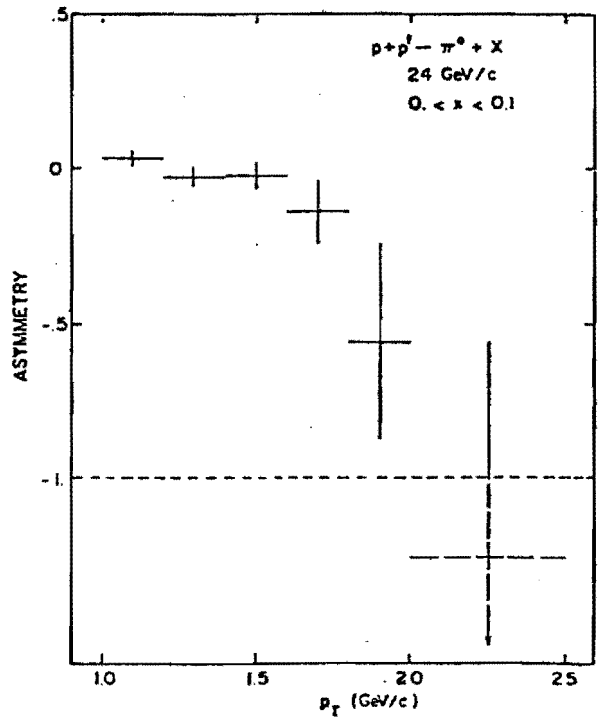

Figure 3

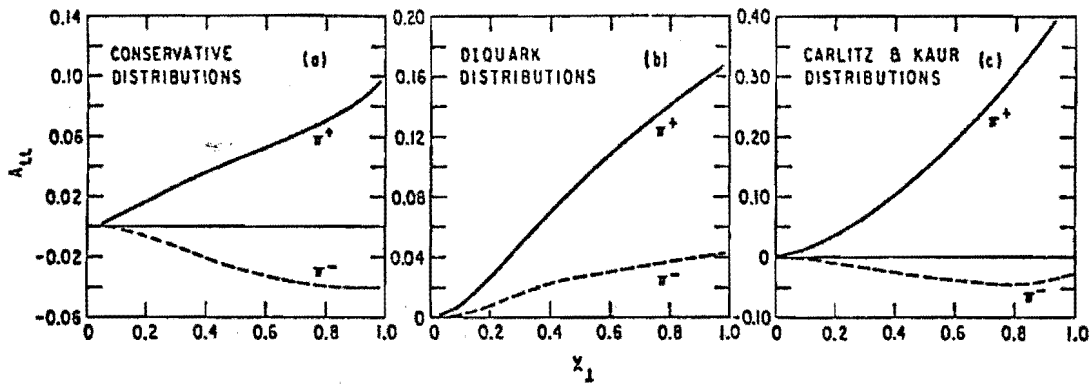
CONSERVATIVE DISTRIBUTIONS
(a)
DIQUARK DISTRIBUTIONS
(b)
CARLITZ & KAUR DISTRIBUTIONS
(c)
π^+
π^-
A_{LL}
$x_\perp$
0.14
0.10
0.06
0.02
-0.02
-0.06
0.20
0.16
0.12
0.08
0.04
0
0.40
0.30
0.20
0.10
0
-0.10
0
0.2
0.4
0.6
0.8
1.0

Figure 4

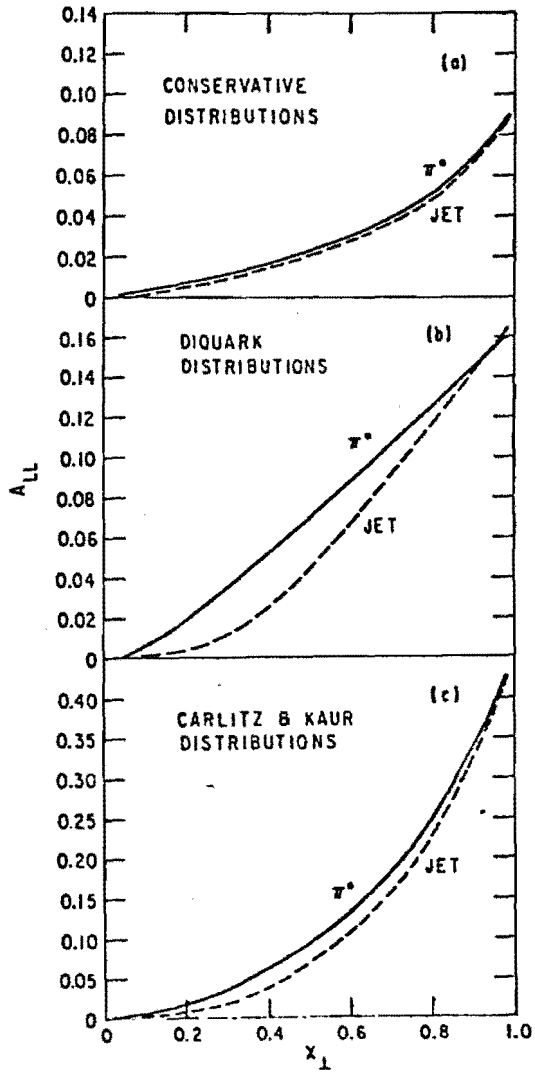
0.14
0.12
0.10
0.08
0.06
0.04
0.02
0
(a)
CONSERVATIVE
DISTRIBUTIONS
π°
JET
0.16
0.14
0.12
0.10
0.08
0.06
0.04
0.02
0
(b)
DIQUARK
DISTRIBUTIONS
π°
JET
A_{LL}
0.40
0.35
0.30
0.25
0.20
0.15
0.10
0.05
0
(c)
CARLITZ & KAUR
DISTRIBUTIONS
π°
JET
0
0.2
0.4
0.6
0.8
1.0
$x_\perp$

Figure 5

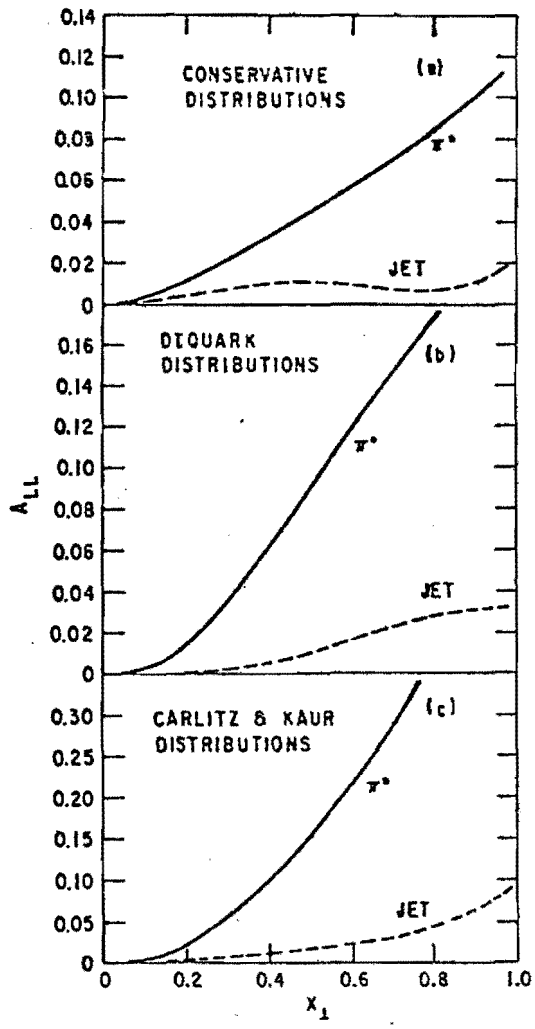
CONSERVATIVE DISTRIBUTIONS
(a)
π°
JET
DIQUARK DISTRIBUTIONS
(b)
π°
JET
CARLITZ & KAUR DISTRIBUTIONS
(c)
π°
JET
A_{LL}
$x_\perp$
0.14
0.12
0.10
0.08
0.06
0.04
0.02
0
0.16
0.14
0.12
0.10
0.08
0.06
0.04
0.02
0
0.30
0.25
0.20
0.15
0.10
0.05
0
0
0.2
0.4
0.6
0.8
1.0

Figure 6

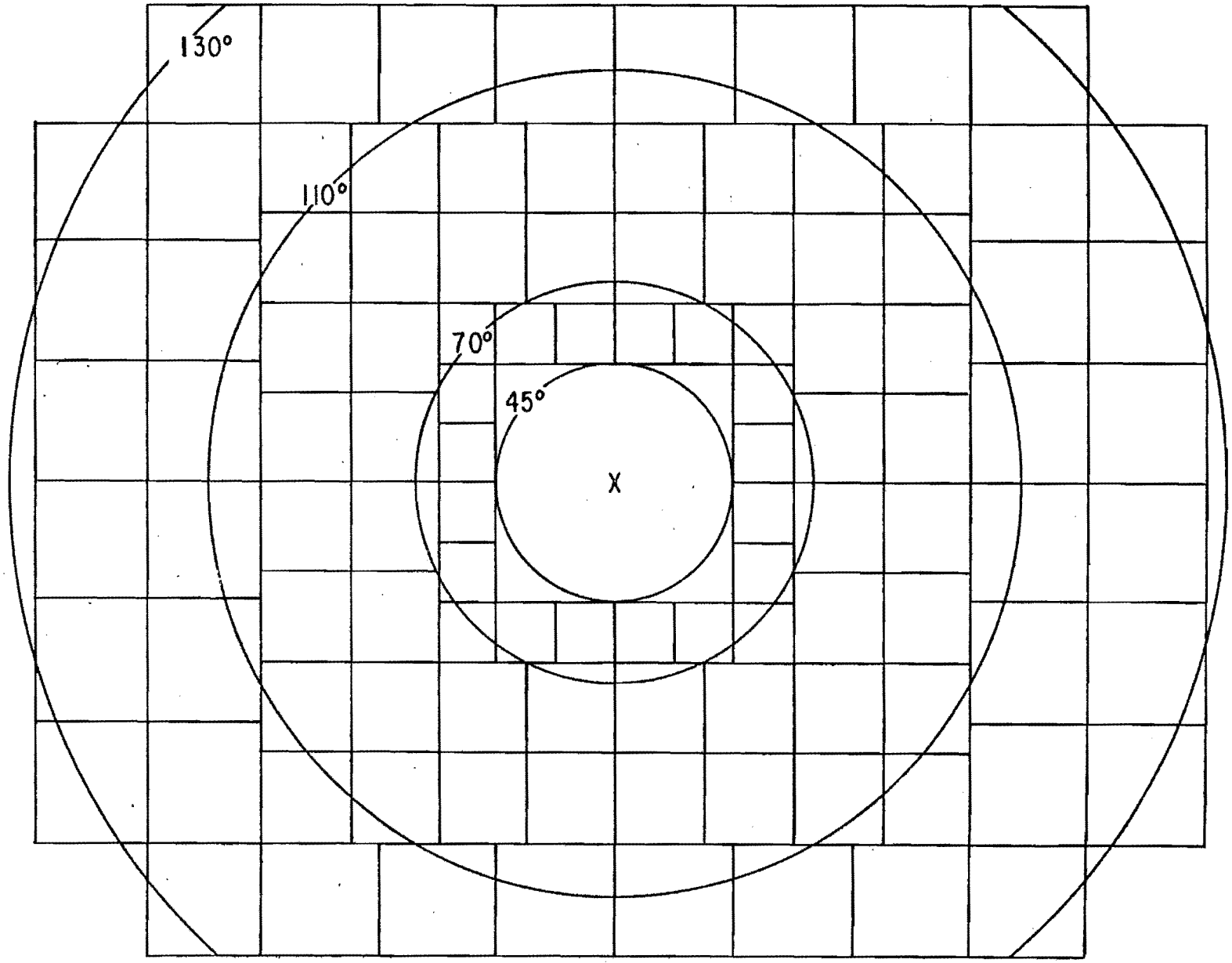

Figure 7

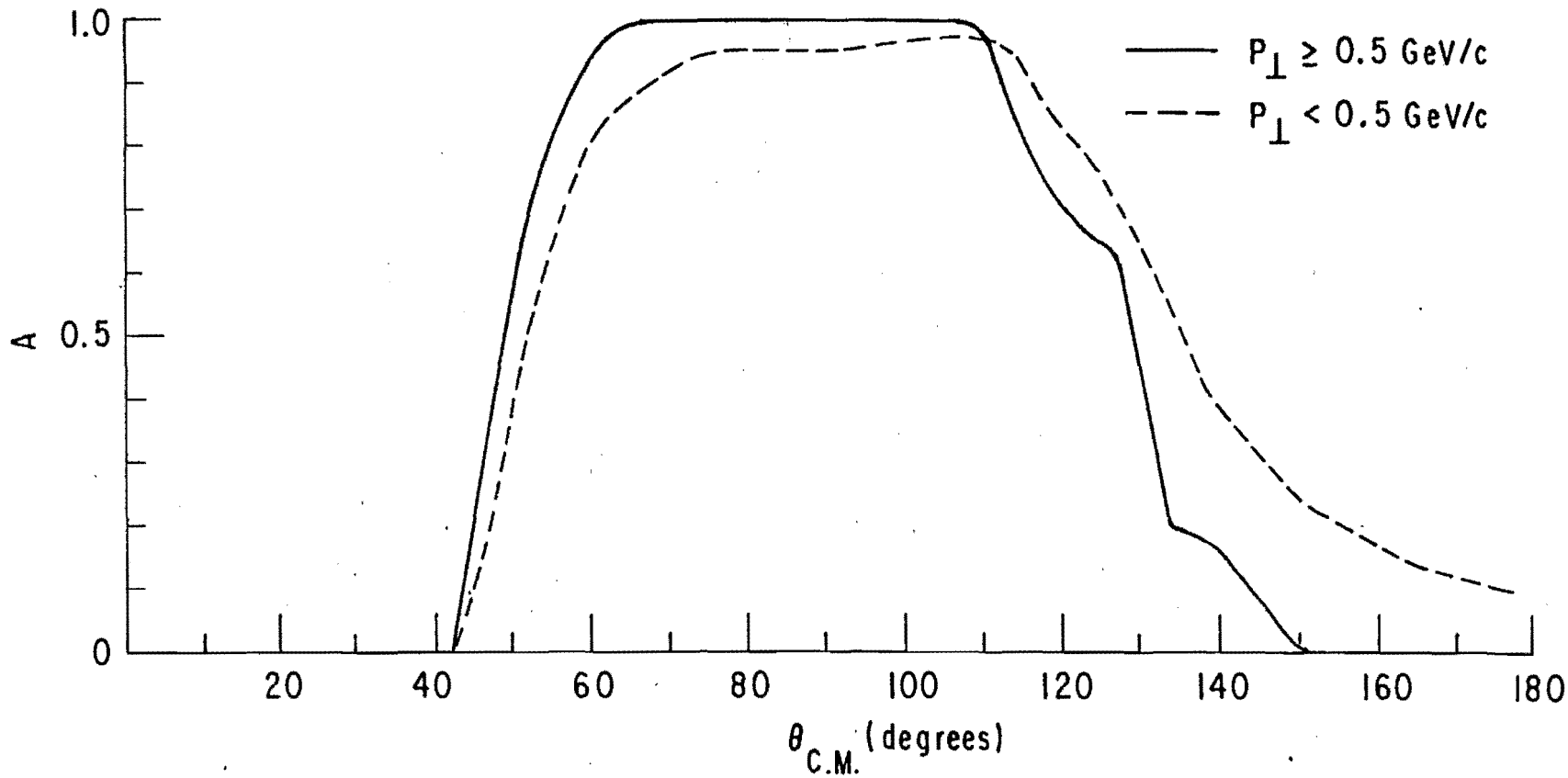
1.0
0.5
0
A
20
40
60
80
100
120
140
160
180
$\theta_{C.M.}$ (degrees)
$P_\perp \geq 0.5$ GeV/c
$P_\perp < 0.5$ GeV/c

Figure 8

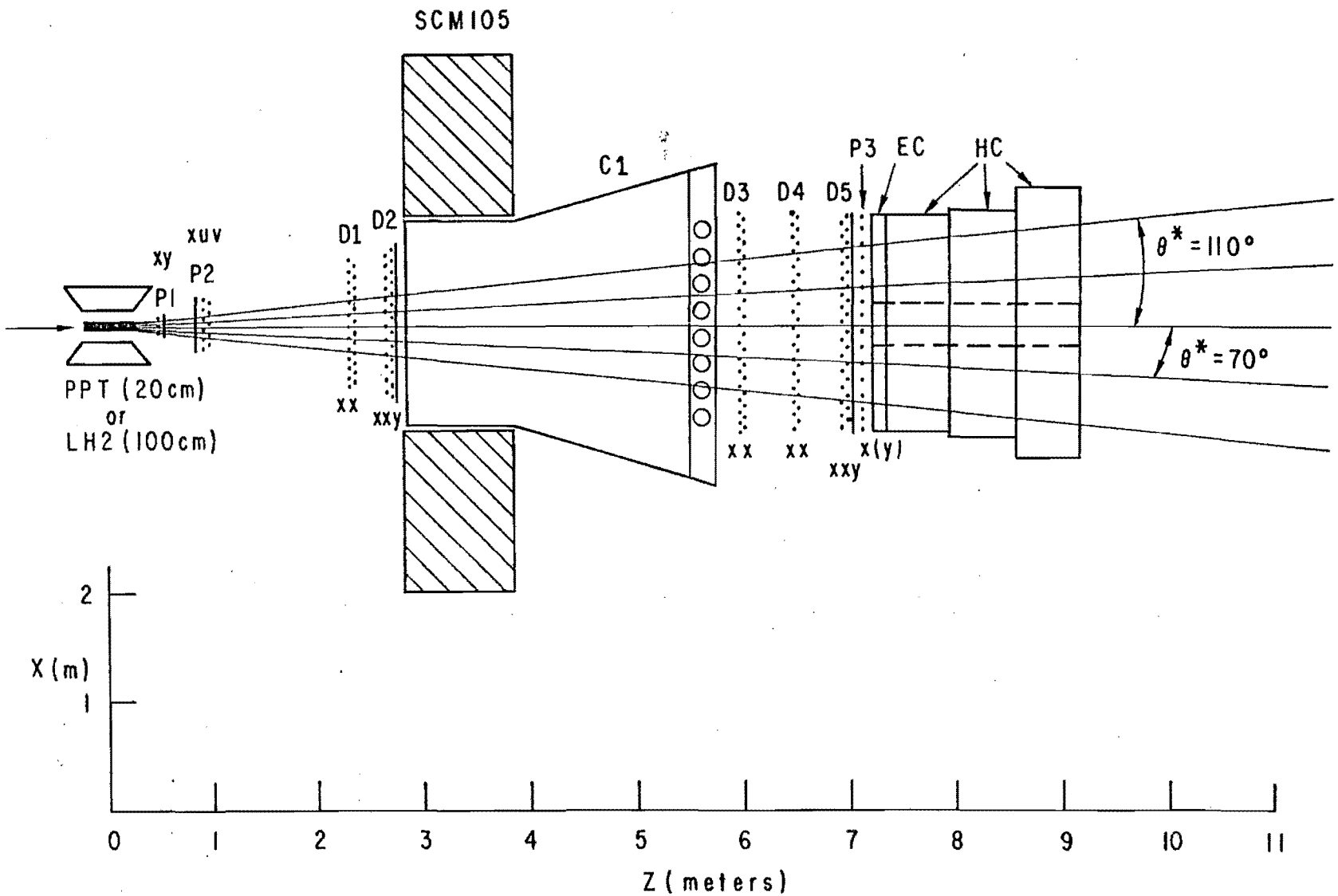
SCM105
C1
D1
D2
D3
D4
D5
P3
EC
HC
xuv
xy
P2
P1
PPT (20cm)
or
LH2 (100cm)
xx
xxy
xx
xx
xxy
x(y)
θ* = 110°
θ* = 70°
X (m)
2
1
0
1
2
3
4
5
6
7
8
9
10
11
Z (meters)

Figure 9

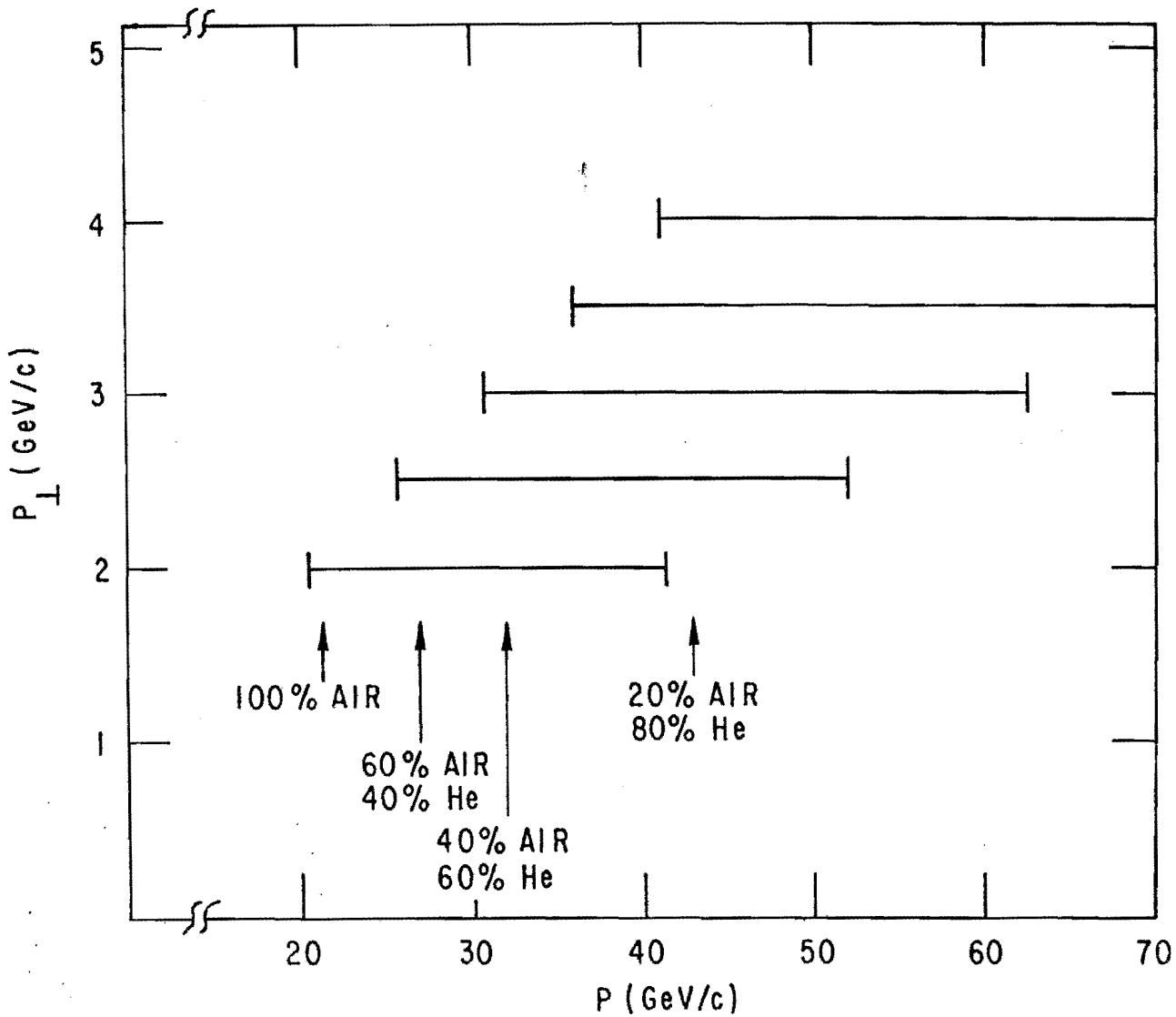
5
4
3
2
1
$P_\perp$ (GeV/c)
100% AIR
60% AIR
40% He
40% AIR
60% He
20% AIR
80% He
20
30
40
50
60
70
P (GeV/c)

Figure 10

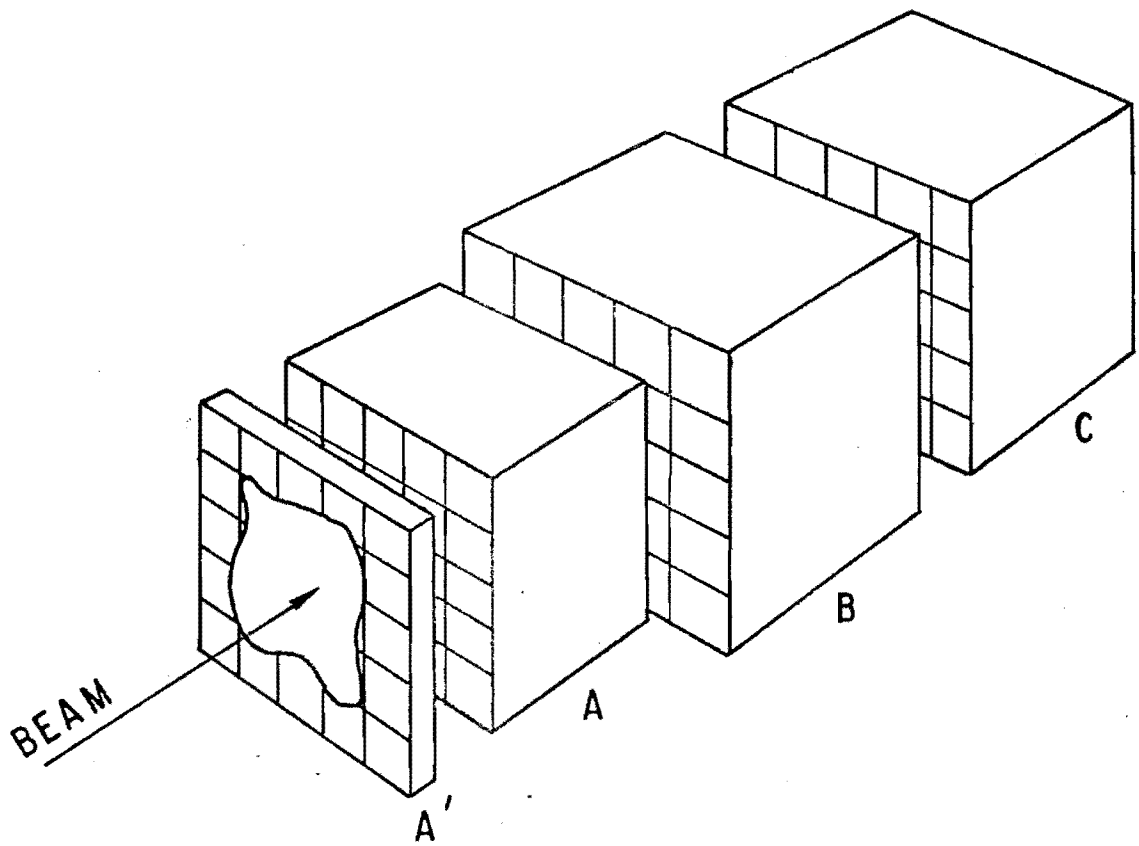

Figure 11

Appendix 1

Table of 1st-Order QCD Cross Sections for Pure-Helicity States

(All cross sections are to be multiplied by a common factor $\pi\alpha_s{}^2/s^2$.)

Process $ab \to cd$	$d\sigma/dt(a(+)b(+) \to cd)$	$d\sigma/dt(a(+)b(-) \to cd)$
$q_\alpha q_\beta \to q_\alpha q_\beta$	$\frac{8}{9}\left[\frac{s^2}{t^2} + \delta_{\alpha\beta}\left(\frac{s^2}{u^2} - \frac{2}{3}\right)\frac{s^2}{tu}\right]$	$\frac{8}{9}\left(\frac{u^2}{t^2} + \delta_{\alpha\beta}\frac{t^2}{u^2}\right)$
$q_\alpha \bar{q}_\beta \to q_\delta \bar{q}_\gamma$	$\frac{8}{9}\left(\delta_{\alpha\beta}\delta_{\beta\gamma}\frac{s^2}{t^2}\right)$	$\frac{8}{9}\left[\delta_{\alpha\delta}\delta_{\beta\gamma}\frac{u^2}{t^2}\right)$
	$+\delta_{\alpha\beta}\delta_{\delta\gamma}\frac{(t^2+u^2)}{s^2}$	
	$-\frac{2}{3}\delta_{\alpha\gamma}\delta_{\alpha\beta}\delta_{\delta\gamma}\frac{u^2}{st}\Big]$	
$qG \to qG$	$\left(\frac{2s^2}{t^2} - \frac{8}{9}\frac{s^2}{us}\right)$	$\left(\frac{2u^2}{t^2} - \frac{8}{9}\frac{u^2}{us}\right)$
$\bar{q}G \to \bar{q}G$	$\left(\frac{2s^2}{t^2} - \frac{8}{9}\frac{s^2}{us}\right)$	$\left(\frac{2u^2}{t^2} - \frac{8}{9}\frac{u^2}{us}\right)$

$GG \to q\bar{q}$	0	$\left[\frac{1}{3}\frac{(u^2+t^2)}{ut} - \frac{3}{4}\frac{(t^2+u^2)}{s^2}\right]$	
$q\bar{q} \to GG$	0	$\left(\frac{64}{27}\frac{t^2+u^2}{ut} - \frac{16}{3}\frac{t^2+u^2}{s^2}\right)$	
$GG \to GG$	$\frac{9}{2}\left(\frac{2s^2}{ut} - \frac{su}{t^2} - \frac{st}{u^2}\right)$		$\frac{9}{2}\left(6 - \frac{2s^2}{ut} - \frac{su}{t^2} - \frac{st}{u^2} - \frac{2ut}{s^2}\right)$

Note: (+) (+) is $\to\leftarrow$, and (+)(−) is $\to\to$.